Heteromeric interactions regulate butyrophilin (BTN) and BTN-like molecules governing γδ T cell biology

Pierre Vantourout[a,b], Adam Laing[a,b], Martin J. Woodward[a,b], Iva Zlatareva[a,b], Luis Apolonia[c], Andrew W. Jones[d], Ambrosius P. Snijders[d], Michael H. Malim[c], and Adrian C. Hayday[a,b,1]

[a]Peter Gorer Department of Immunobiology, King's College London, London SE1 9RT, United Kingdom; [b]Immunosurveillance Laboratory, The Francis Crick Institute, London NW11AT, United Kingdom; [c]Department of Infectious Diseases, King's College London, London SE1 9RT, United Kingdom; and [d]Mass Spectrometry Proteomics Platform, The Francis Crick Institute, London NW11AT, United Kingdom

Edited by Peter Cresswell, Yale University School of Medicine, New Haven, CT, and approved December 19, 2017 (received for review January 23, 2017)

The long-held view that gamma delta (γδ) T cells in mice and humans are fundamentally dissimilar, as are γδ cells in blood and peripheral tissues, has been challenged by emerging evidence of the cells' regulation by butyrophilin (BTN) and butyrophilin-like (BTNL) molecules. Thus, murine *Btnl1* and the related gene, *Skint1*, mediate T cell receptor (TCR)-dependent selection of murine intraepithelial γδ T cell repertoires in gut and skin, respectively; *BTNL3* and *BTNL8* are TCR-dependent regulators of human gut γδ cells; and *BTN3A1* is essential for TCR-dependent activation of human peripheral blood Vγ9Vδ2$^+$ T cells. However, some observations concerning BTN/Btnl molecules continue to question the extent of mechanistic conservation. In particular, murine and human gut γδ cell regulation depends on pairings of Btnl1 and Btnl6 and BTNL3 and BTNL8, respectively, whereas blood γδ cells are reported to be regulated by BTN3A1 independent of other BTNs. Addressing this paradox, we show that BTN3A2 regulates the subcellular localization of BTN3A1, including functionally important associations with the endoplasmic reticulum (ER), and is specifically required for optimal BTN3A1-mediated activation of Vγ9Vδ2$^+$ T cells. Evidence that BTNL3/BTNL8 and Btnl1/Btnl6 likewise associate with the ER reinforces the prospect of broadly conserved mechanisms underpinning the selection and activation of γδ cells in mice and humans, and in blood and extralymphoid sites.

gamma delta T cells | butyrophilins | endoplasmic reticulum | zoledronate | evolutionary conservation

Ever since their unanticipated discovery (1, 2), the T cell receptor (TCR) γ and δ chains and the cells that express them have offered insights into immunology. For example, rather than focusing on discrete, pathogen-specific epitopes (e.g., peptides), γδ TCRs collectively respond to highly diverse antigens, ranging from self-encoded moieties induced by cellular dysregulation through lipids presented by CD1 to microbial molecular patterns (3, 4). Conspicuous among these is the response of most human peripheral blood Vγ9Vδ2$^+$ T cells to low-molecular-mass "phosphoantigens" (PAgs), including hydroxymethyl but-2-enyl pyrophosphate (HMBPP), an intermediate in the deoxyxylulose phosphate pathway in many bacteria and protozoa, and isopentenylpyrophosphate, an intermediate in the mevalonate pathway employed from bacteria through to vertebrates and commonly overexpressed by virus-infected cells or cells transformed by p53 inactivation (5, 6). How such charged, low-molecular-mass molecules activate signaling from large, cell-surface TCR complexes is unclear, fueling the search for a presenting element, akin to CD1.

In that regard, PAg activation of Vγ9Vδ2$^+$ T cells requires *BTN3A1* (7), a member of the butyrophilin (*BTN*) and BTN-like (*BTNL*) family that in humans comprises 11 genes related to those encoding "B7-superfamily" members, including PD-L1. The *BTN3A1* gene lies close to *BTN3A2* and *BTN3A3*, and all three encode type 1 transmembrane proteins comprising an Ig variable (V) and Ig constant (C) region linked via a single pass transmembrane (TM) domain to an intracellular region that in BTN3A1 and BTN3A3 includes a B30.2 domain, akin to that found in many BTN(L) and TRIM proteins (8).

BTN3A1 forms homodimers (9) and was reported to bind PAg via its extracellular IgV domain, thereby presenting it directly to the Vγ9Vδ2 TCR (10). However, this mechanism for PAg-dependent, TCR-mediated γδ cell activation failed to explain why BTN3A2 seemingly could not present PAg, despite its identical IgV domain. Moreover, others have reported PAg binding to the intracellular B30.2 domain, within which histidine 381 appeared particularly important (11–13). Sensing of intracellular PAg levels by BTN3A1 was shown to alter the conformation of its B30.2 domain (14, 15), although how this might trigger Vγ9Vδ2$^+$ T cell activation remains unclear, as the PAg site can also bind biologically inactive negatively charged molecules (15).

Provocatively, the implication of BTN3A1 in Vγ9Vδ2 T cell activation followed the earlier demonstration that the murine *Btnl* gene, *Skint1*, drives the selective development of murine intraepidermal Vγ5Vδ1$^+$ T cells (16–18). Furthermore, we recently showed that murine *Btnl1*/*Btnl6* drive the selective development of murine intestinal Vγ7$^+$ intraepithelial T cells, whereas human *BTNL3*/*BTNL8* selectively regulate human gut Vγ4$^+$ T cells (19). Thus, a general role is emerging for BTN/BTNL in γδ cell biology.

However, the notion of broadly conserved mechanisms of γδ cell regulation is challenged by the fact that TCR-dependent mouse and human gut γδ cell regulation requires pairings of proteins encoded by *Btnl1*/*Btnl6* and *BTNL3*/*BTNL8*, respectively, whereas there is conflicting evidence as to whether Vγ9Vδ2$^+$ T cell regulation by BTN3A1 also requires BTN3A2 and/or BTN3A3 (7, 10, 13). Addressing this paradox, our study shows that BTN3A2 regulates

Significance

Although gamma delta (γδ) T cells compose an evolutionarily conserved third lineage of diversified lymphocytes, alongside αβ T cells and B cells, they can seem overtly different across species and tissues. Thus, human blood γδ cells show butyrophilin (BTN)3A1-dependent responses to metabolites ("phosphoantigens") not seen by rodent γδ cells, whereas some rodent, γδ-rich compartments, notably in the skin, lack obvious human counterparts. Recently, however, mouse and human intraepithelial gut γδ cells were found to be regulated by pairings of BTN-like genes. This study now shows that BTN3A1 also functions as a pairing, with its subcellular trafficking and optimal activity both regulated by BTN3A2. Hence, seemingly diverse γδ cell biologies across species and tissues are underpinned by conserved mechanisms.

Author contributions: P.V. and A.C.H. designed research; P.V., A.L., M.J.W., I.Z., L.A., and A.W.J. performed research; P.V., A.L., M.J.W., L.A., A.P.S., M.H.M., and A.C.H. analyzed data; and A.C.H. wrote the paper.

The authors declare no conflict of interest.

This article is a PNAS Direct Submission.

[1]To whom correspondence should be addressed. Email: adrian.hayday@kcl.ac.uk.

This article contains supporting information online at www.pnas.org/lookup/suppl/doi:10.1073/pnas.1701237115/-/DCSupplemental.

the subcellular localization of BTN3A1, including association with the ER, and is essential for the optimal activation of Vγ9Vδ2$^+$ T cells. Likewise, we find that BTNL3/BTNL8 and Btnl1/Btnl6 are ER-associated. Hence, conserved molecular mechanisms seemingly underpin the regulation of major γδ cell subsets across mice and humans, and across blood and extralymphoid tissues.

Results

Vγ9Vδ2 T Cell Activation Requires BTN3A1 and BTN3A2. Human HEK293T (293T) embryonic kidney epithelial cells readily stimulate Vγ9Vδ2$^+$ T cells when pulsed with either HMBPP or zoledronate (Zol), a clinically used aminobisphosphonate that induces isopentenylpyrophosphate accumulation by inhibiting farnesyl pyrophosphate synthase (20). Vγ9Vδ2$^+$ T cell stimulation is routinely assayed by increased surface expression of CD107a (LAMP-1), reflecting exocytotic degranulation of cytolytic lysosomes (Fig. S1*A*). Consistent with expression by many cell types, RNAs for all *BTN3A* genes were expressed by 293T cells (Fig. S1*B*), and pan anti-BTN3A antibody (monoclonal antibody 20.1), which cannot discriminate among the three proteins, detected cell surface BTN3A, as it did on peripheral blood cell subtypes of three healthy donors (Fig. S1 *C* and *D*).

To assess the contributions of BTN3A1, BTN3A2, and/or BTN3A3 with Vγ9Vδ2$^+$ T cell stimulation (Fig. 1*A*), we generated 293T lines with disruptions of *BTN3A1* (CRA1), *BTN3A2* (CRA2), *BTN3A3* (CRA3), all three genes (CRA123), and *BTN3A2+3A3* (CRA23; Fig. S2*A*), which we validated by failure to amplify full-length products of the relevant *BTN3A* genes (Fig. 1*B*) and diminished anti-BTN3A antibody staining (Fig. S2*B*). Consistent with deleting the *BTN3A* cluster, CRA123 cells also showed disrupted *BTN2A2* expression (Fig. 1*B*). Control cells (CREV) were transfected with CRISPR (CR)/Cas9 lacking *BTN* targeting sequences.

The cell lines were pulsed with a dose-range of Zol and assessed for their activation of Vγ9Vδ2$^+$ T cells. CREV showed a potency (E_{max}) of ∼70% of Vγ9Vδ2$^+$ T cells degranulating, with EC_{50} of <1 μM Zol (Fig. 1*C* and Fig. S2*C*). As expected, this capacity was completely lost from cells with disrupted *BTN3A1*, either alone (CRA1) or along with *BTN3A2* and *BTN3A3* (CRA123) (Fig. 1*C* and Fig. S2*C*). Hence, *BTN3A1* is, as described, strictly required for Vγ9Vδ2$^+$ T cell activation (7, 10, 11, 13). Conspicuously, CRA2 cells that express endogenous *BTN3A1* but lack *BTN3A2* also showed impaired activation of Vγ9Vδ2$^+$ T cells (Fig. 1*C* and Fig. S2*C*). Although the EC_{50} for CRA2 cells was also ∼1.0 μM Zol, potency was reduced by ∼50%. Moreover, CRA23 cells that also express *BTN3A1* but neither *BTN3A2* nor *BTN3A3* did not activate Vγ9Vδ2$^+$ T cells (Fig. 1*C* and Fig. S2*C*). Conversely, CRA3 cells lacking only BTN3A3 functioned comparably to CREV cells. In sum, the full functional activity of BTN3A1 required BTN3A2, with some capacity of BTN3A3 to substitute for BTN3A2. This perspective was reinforced by experiments in which the functional rescue of CRA123 cells by single *BTN3A* genes and combinations thereof was attempted across a range of Zol concentrations. CRA123 cells transfected with *BTN3A2*, *BTN3A3*, or *BTN3A2+A3* showed residual functional capacity. Conversely, CRA123 cells rescued with BTN3A1+3A2 or BTN33A1+3A3 showed EC_{50} and E_{max} comparable to control cells (CREV), whereas cells transfected with only BTN3A1 showed greatly increased EC_{50} (Fig. 1*D* and Fig. S2*D*). Thus, BTN3A1 is necessary but insufficient to promote optimal, Zol-dependent, Vγ9Vδ2$^+$ T cell activation.

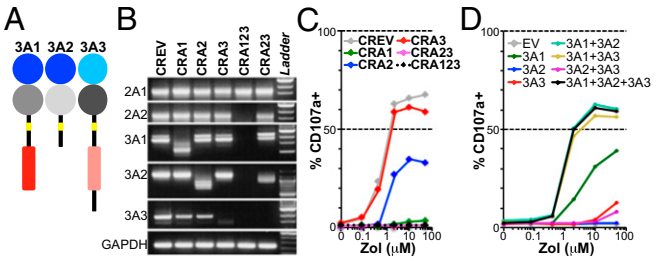

Fig. 1. Requirements for BTN3 proteins for Vγ9Vδ2$^+$ T cell responses to PAgs. (*A*) Schematic domain organization of BTN3A proteins (blue, IgV; gray, IgC; yellow, TM; red/pink B30.2 domain). (*B*) RT-PCR for the *BTN* genes listed on the left and for *GAPDH*, using RNA of denoted cell lines (*Upper*). (*C*) Cell lines listed were pulsed for 12 h with Zol (0.04–50 μM, 5× dilution steps) and cocultured for 5 h with a polyclonal Vγ9Vδ2$^+$ T cell line in the presence of a CD107a antibody: results are means of duplicate stimulations, representative of two independent experiments. (*D*) CRA123 cells were transfected with pCSIGPW, either EV or encoding the indicated BTN3 proteins, single or in combinations, before treatment with Zol and assayed for their capacity to promote Vγ9Vδ2$^+$ T cell degranulation as in *C*.

BTN3A1 Heteromers. To assess how BTN3A proteins might collaborate, we focused on their potential to interact. Because BTN3A1 can homodimerize via its IgC domain (9), we considered that BTN3A proteins might similarly form heteromers. Indeed, heterodimers of BTN3A1 and BTN3A2 produced in high quantities in insect cells were recently visualized by electron microscopy, although they were not studied in detail (14). Thus, N-terminal FLAG-tagged BTN3A1 was expressed in CRA123 cells with or without N-terminal HA-tagged BTN3A2, or HA-3A2ΔIgC that lacks the IgC domain. Anti-FLAG- and anti-HA-reactive bands of appropriate molecular mass were detected as input proteins by Western blotting lysates from singly- and doubly-transfected cells (Fig. 2*A*, *Left*; Hsp90, loading control). Importantly, anti-HA also detected HA-BTN3A2, but not HA-3A2ΔIgC, in anti-FLAG immunoprecipitates of doubly-transfected cells (Fig. 2*A*, *Right*). Thus, BTN3A2 complexed with BTN3A1 in an IgC-dependent manner. This was further investigated via mass spectrometry. By plotting protein intensity ratios (Welch Difference) versus log10 sum of intensities, BTN3A1 was, as expected, the most greatly enriched high-intensity species in anti-FLAG immunoprecipitates from cells cotransduced with FLAG-3A1+HA-3A2 versus cells transduced with empty vector (Fig. 2*B*). Of note, however, there was stoichiometric enrichment of BTN3A2. Because no other moiety was likewise enriched, complexes likely reflect direct, 1:1 interactions of BTN3A1 and BTN3A2, without stoichiometric mediation by a third party, consistent with the visualization of complexes obtained using purified BTN3A1 and BTN3A2 proteins (14).

BTN3A3 could also be coimmunoprecipitated with BTN3A1 (Fig. S3*A*), consistent with its potential to functionally collaborate with BTN3A1 in the absence of BTN3A2 (Fig. 1*D*). However, BTN3A1 did not coimmunoprecipitate HA-BTNL8, which coregulates human gut γδ cells, together with BTNL3 (Fig. S3*B*). Indeed, FLAG-BTNL3 coimmunoprecipitated HA-BTNL8, but not HA-BTN3A2 or HA-BTN3A3. Mass spectrometry revealed statistically significant coenrichment of BTNL3+8 in anti-FLAG BTNL3 immunoprecipitates, again without obvious coenrichment of a third party (Fig. 2*B* and Fig. S3*C*). Thus, BTN3A1+3A2 and BTNL3+L8, respectively, form complexes with shared features.

Coregulation of Cell Localization. Next, we used flow cytometry to assess how the potential to form complexes might regulate BTN3A1. When CRA123 cells were transfected with the corresponding genes upstream of an internal ribosome entry site (IRES)-GFP reporter, GFP fluorescence intensity was largely proportional to total protein levels of each BTN3A gene product, as measured 24 h posttransfection by flow cytometry of permeabilized cells (Fig. S4*A*). However, nonpermeabilized *BTN3A1*-transfected cells lacked such proportionality, whether measured at 12, 24, or 48 h posttransfection; indeed, only GFP^{hi} cells (indicative of extreme *BTN3A1* overexpression) displayed surface BTN3A1 expression (Fig. 2*C* and Fig. S4*A*). Hence, BTN3A1 was intrinsically inefficient at cell surface localization. Conversely, BTN3A3 was more efficient at cell surface localization, whereas BTN3A2 showed intermediate properties (Fig. 2*C* and Fig. S4*A*). The distinct phenotypes were not a result of minor differences in leader-peptide (LP) sequences, as swapping those across BTN3A proteins (e.g., LP^{3A2}-3A1, LP^{3A1}-3A3) did not affect the signature

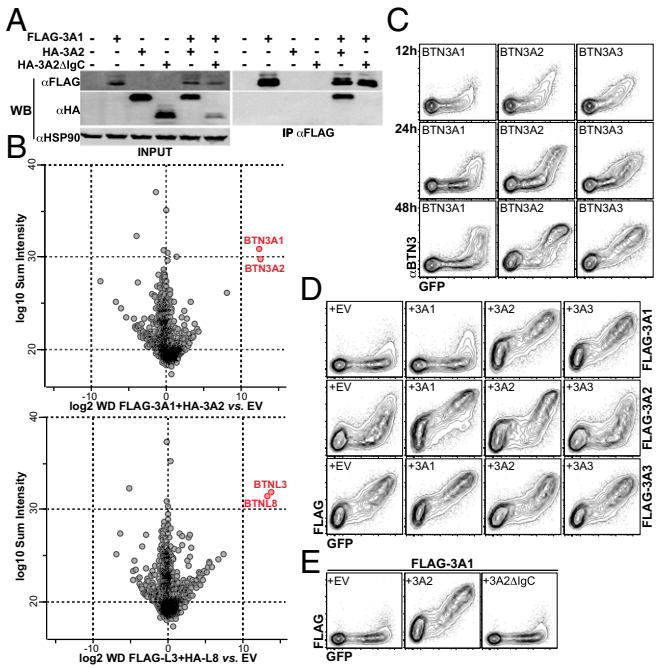

Fig. 2. Heteromeric interactions regulate BTN3 surface expression. (*A*) CRA123 cells were lysed 48 h posttransfection with the indicated constructs (*Upper*); one fraction was used to measure total protein expression (INPUT), and the remainder was immunoprecipitated with protein G beads coated with an anti-FLAG antibody (IP). Samples were loaded onto 12% SDS/PAGE and analyzed by Western blot (WB) with the indicated antibodies. Representative of three experiments. (*B*) IP-MS volcano plot of protein intensity ratios comparing anti-FLAG pull-downs performed on lysates from CRA123 cells transduced with FLAG-BTN3A1+HA-BTN3A2 versus EV control (*Top*) or FLAG-BTNL3+HA-BTNL8 versus EV (*Bottom*). *X*-axis: log2 LFQ protein intensity ratios (Welch Difference); *y* axis: log10 sum of intensities. (*C*) CRA123 cells were transfected with the indicated constructs and BTN3 expression assessed by flow cytometry (with anti-pan-BTN3A) 12, 24, or 48 h later. Representative of five independent experiments. (*D* and *E*) CRA123 cells were cotransfected with FLAG-tagged constructs (indicated on the right-hand side) and WT constructs (indicated in each quadrant). Anti-FLAG-reactive proteins expression was assessed by flow cytometry 24 h posttransfection. Representative of five independent experiments.

expression patterns (Fig. S4*B*), which were also unaltered in Zol-pulsed or HMBPP-pulsed cells. Surface expression of N-terminal FLAG-tagged BTN3A1 was greatly enhanced by coexpression with untagged BTN3A2 or BTN3A3 (Fig. 2*D*, *Upper*). Conversely, BTN3A3 did not enhance surface BTN3A2 expression (Fig. 2D, *Middle*). Consistent with its failure to coimmunoprecipitate with BTN3A1 (Fig. 2*A*), BTN3A2ΔIgC did not promote surface BTN3A1 expression (Fig. 2*E*). BTN3A1 surface expression was likewise not promoted by BTN1A1, BTN2A1, BTN2A2, BTNL3, BTNL8, or BTNL8-short (BTNL8S; Fig. S5*A*), further attesting to the specificity of BTN3A protein interactions.

To independently analyze BTN3A1 expression, confocal microscopy was employed. On cells coexpressing FLAG-BTN3A1 and HA-BTN3A2ΔIgC (which cannot interact with each other), anti-HA detected some surface expression of BTN3A2ΔIgC, but anti-FLAG only detected BTN3A1 in permeabilized cells (Fig. S5*B*). In contrast, nonpermeabilized cells coexpressing FLAG-BTN3A1 and HA-BTN3A2 [which can complex (Fig. 2*A*)] stained for both FLAG and HA, reflecting the proteins' coexpression and cell surface colocalization (Fig. S5*B*). Taken together, the data argue that IgC-dependent interactions of BTN3A1 and BTN3A2 regulate their subcellular localization. To investigate the molecular basis for this functional collaboration, an extended mutational analysis was undertaken of BTN3A1 and BTN3A2, as these (unlike BTN3A3) were each required for full PAg-dependent T cell activation (Fig. 1*C*).

Motifs Within BTN3A1. CRA123 cells (lacking all *BTN3A* genes) were transfected with a set of BTN3A1 chimaeras (Fig. 3*A*) and assessed for surface expression and the corresponding capacity to stimulate Vγ9Vδ2$^+$ T cells. Relative to BTN3A1, BTN3A3 possesses an extended C terminus beyond the B30.2 domain, and when this was added to BTN3A1 (3A1-3, Fig. 3*A*, purple), it improved its surface expression (Fig. 3*B*). Given that the C terminus can evidently modify the subcellular localization of BTN3A proteins, we generated a chimaera fusing GFP to the C terminus of BTN3A1 (3A1-GFP), a strategy employed by others (7, 14). This too showed greatly increased BTN3A1 surface expression (Fig. 3 *A* and *B*, green), suggesting caution in interpreting data where C-terminal BTN3A fusions are used interchangeably with wild type. Increased surface BTN3A1 expression was also achieved by substituting the intracellular region (Gln_{272}-Lys_{334}) located between the TM and B30.2 domains of BTN3A1 with the corresponding region (Arg_{272}-Ala_{334}) of BTN3A2 (3A1/2-1; Fig. 3 *A* and *B*, blue). When assayed for their functional potentials using a standard concentration of Zol (5 μM), greatly increased surface expression invariably decreased PAg-dependent Vγ9Vδ2$^+$ T cell activation, the most extreme example being 3A1/2-1 (Fig. 3*C* and Fig. S6*A*). Hence, subcellular localization profoundly affected BTN3A1 function, as is further considered here.

Because the 3A1/2-1 construct includes the BTN3A1 ectodomain and the B30.2 domain, including His381, its failure to drive Vγ9Vδ2$^+$ T cell activation implicates the region (Gln_{272}-Lys_{334}) as critical for function. Indeed, placing the entire intracellular region (Gln_{272}-Ala_{513}) of BTN3A1 downstream of the BTN3A2 ecto- and TM-domains (3A2/1) fully recapitulated the signature expression and function of BTN3A1 (Fig. 4 *A*–*C*), clearly demonstrating that the BTN3A1 and BTN3A2 extracellular domains are interchangeable. In contrast, a construct (3A2-1) in which just the BTN3A1 C terminus (Ala_{335}-Ala_{513}), including the B30.2 domain, was directly fused to the C terminus of BTN3A2 displayed increased surface expression relative to BTN3A1, but no function (Fig. 4 *A*–*C*), providing further evidence that BTN3A1 function depends on intracellular determinants lying between its TM and B30.2 domains, located between Gln_{272} and Lys_{334}.

Motifs Within BTN3A2. To define BTN3A2 sequences required to functionally collaborate with endogenous BTN3A1, we employed CRA23 cells that express *BTN3A1*. Consistent with data presented earlier, functional rescue was achieved by reexpression of *BTN3A2*, but not *BTN3A2ΔIgC*, whose gene-product cannot associate with BTN3A1 (Fig. 4 *D* and *E* and Fig. S6*B*). Thereupon, we focused on the relatively short intracellular domain of BTN3A2, which lacks a B30.2 domain (Fig. 1*A*). Removal of the 20 most C-terminal amino acids (3A2Δ315–334) prevented BTN3A2 from functionally rescuing CRA23 cells, whereas truncation of the last 10 amino acids (3A2Δ325–334) did not (Fig. 4 *D* and *E* and Fig. S6*B*), thus establishing the importance of amino

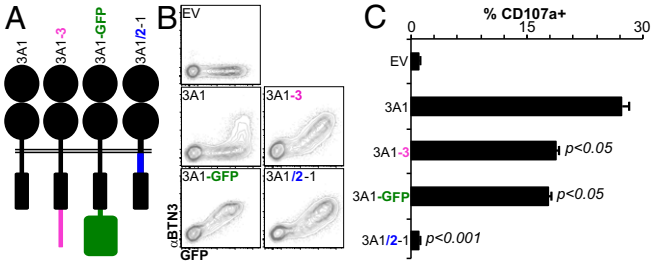

Fig. 3. BTN3A1 surface expression versus functional competence. (*A*) Schematic representation of the BTN3A1 constructs used to transfect CRA123 cells before treatment with 5 μM Zol. (*B*) Expression was monitored by flow cytometry on a fraction of the samples, whereas the remainder (*C*) was coincubated with Vγ9Vδ2$^+$ cells in the presence of an anti-CD107a antibody to assay function. Data are means of three stimulations ± SD. Representative of three independent experiments. *P* values are relative to 3A1.

acids 315–324. This decamer includes KRKKIQ$_{313–318}$, which includes two candidate motifs (KxK and KKxx) for ER retention/retrieval, a quality control step influencing the export of properly assembled protein complexes (21, 22). Of note, two different motifs with analogous functional potentials (RWR$_{313–315}$, RGER$_{322–325}$; Fig. 4*F*, purple) are found between the BTN3A1 TM domain (Fig. 4*F*, yellow) and the B30.2 domain (Fig. 4*F*, red) in the Gln$_{272}$-Lys$_{334}$ subregion, shown earlier to be functionally important. Hence, we further investigated these motifs.

ER Association of BTN3A1 and BTN3A2. We first assessed whether the intracellular domains of BTN3A1 and BTN3A2 did contribute to ER retention/retrieval. FLAG-tagged BTN3A1 introduced into CRA123 cells largely colocalized with the ER marker, protein disulphide isomerase (PDI), but not with a Golgi marker, Gm130 (Fig. 5*A*), quantitated by high bright detail similarity (BDS) of FLAG-PDI, but not of FLAG-Gm130 (Fig. 5*A*, *Lower*). Just as BTN3A2 enhanced BTN3A1 surface expression (Fig. 2*D*), BTN3A1 showed reduced ER colocalization in cells cotransfected with BTN3A2 (Fig. 5*A*, orange segregation from cyan; reduced FLAG-PDI BDS). Confocal microscopy likewise revealed that mCherry-tagged Sec61β, another ER-resident marker, colocalized with cotransfected BTN3A1 or BTN3A2 expressed singly, but less so when BTN3A1 and BTN3A2 were coexpressed (Fig. 5*B*).

Consistent with ER association being driven by each of the putative motifs in BTN3A1 and BTN3A2 (Fig. 4*F*), their nonconservative mutation (BTN3A1: RWR$_{313–315}$-RGER$_{322–325}$ > AWA-AGEA, and BTN3A2: KRKKIQ$_{313–318}$ > KRAAIQ) substantially increased the proteins' cell surface expression, whereas conservative R/K substitutions (RWR-RGER > KWK-KGEK) did not, in one case exaggerating BTN3A2 retention (KRKKIQ > KRRRIQ) (Fig. 6*A*).

Given that subcellular localization is critical for function, we considered how the ER retention motifs might affect the proteins' functional collaboration. If expressed with either wild-type BTN3A2 (KRKKIQ) or a KRRRIQ mutant, both of which strongly associate with the ER (Fig. 6*A*), nonconservative mutation of BTN3A1 RWR$_{313–315}$-RGER$_{322–325}$ to AWA-AGEA did not limit functional collaboration, whereas it impaired functional collaboration with the KRAAIQ mutant (Fig. 6 *B* and *C*, purple box and arrow; Fig. 6*D*). Conversely, rescue of the BTN3A1 AWA-AGEA mutant was not significantly reduced by nonconservative mutations of the putative KRK$_{312–314}$ motif (e.g., KRKKIQ > AAKKIQ; Fig. S7). Of note, the BTN3A2-KRAAIQ mutant could still collaborate with either BTN3A1 (WT, RWR-RGER) or the conservative KWK-KGEK mutant (Fig. 6 *B–D*). These data demonstrate complementation, whereby function requires an ER retention motif or motifs in at least one of BTN3A1 or BTN3A2, consistent with the active functional unit being a heteromer with strictly regulated subcellular trafficking. Indeed, it was again the case that some BTN3A1/BTN3A2 mutant pairings (e.g., 3A1-KWK-KGEK+ 3A2-KRRRIQ) were functional despite decreased cell surface expression (Fig. 6*B*, *Right* and Fig. 6 *C* and *D*).

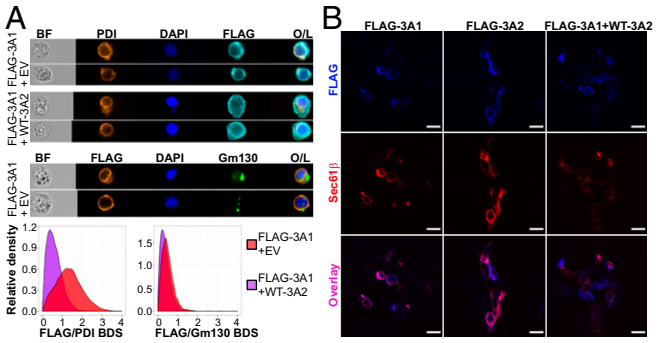

Fig. 5. BTN3A1 and BTN3A2 associate with the ER and regulate each other's trafficking. (*A*) CRA123 cells were transfected with the indicated constructs (*Left*) and permeabilized and stained with anti-FLAG-APC/anti-PDI-PE (ER marker) or anti-FLAG-PE/anti-Gm130-APC (Golgi marker) 48 h posttransfection. Data were acquired on ImageStreamX and processed in IDEAS, and histograms were generated in R. Representative of three independent experiments. BDS, colocalization score; BF, bright field; O/L, overlay. (*B*) CRA123 cells were cotransfected with the indicated BTN3 constructs and mCherry-tagged Sec61β. Cells were permeabilized 48 h posttransfection, stained with anti-FLAG, and analyzed by confocal microscopy. (Scale bars, 20 μm.)

Conserved ER Retention of BTNL/Btnl Proteins. Given the importance of regulated subcellular localization and ER associations for BTN3A1-BTN3A2 collaboration, we examined whether similar properties might underpin Btnl1-Btnl6 and BTNL3-BTNL8 collaborations. After transfection of 293T cells that do not ordinarily express these four proteins, all showed strong PDI colocalization (Fig. S8 *A–D*). Moreover, Btnl1/Btnl6 coexpression reduced PDI colocalization (Fig. S8 *A* and *B*), as was observed for BTN3A2-BTN3A1 collaboration (Fig. 5*A*). Although this was a priori less apparent for BTNL3/BTNL8 coexpression (Fig. S8 *C* and *D*), the effect of coexpression became clearer when asking whether a protein sat within or outside of a "mask" defined by PDI expression: clearly BTNL3/BTNL8 coexpression increased the fraction of protein outside the mask, albeit to a lesser extent than Btnl1/Btnl6 coexpression (Fig. S9*A*). Consistent with this, BTNL8 coexpression increased BTNL3 surface expression (Fig. S9*B*; compare the green histograms). In sum, all BTN(L)/Btnl proteins implicated in specific γδ subset regulation displayed hallmarks of preferential ER association that were diminished by coexpression of their functionally relevant partners.

Further Functional BTN/BTNL/Btnl Conservation. Finally, another short subregion between the TM and B30.2 domains of BTN3A1 (YNEWKKALFKPA), recently found to be functionally important (23), is centered on an EWK motif that we also found to be functionally indispensable for Vγ9Vδ2$^+$ cell activation (Fig. S9*C*). However, it was unaffected by mutation to DWR, which is conserved similarly close to the B30.2 domains of BTNL3, BTNL8, Btnl1, and Btnl6 (Fig. S9*D*), providing further indications of conservation of mechanism.

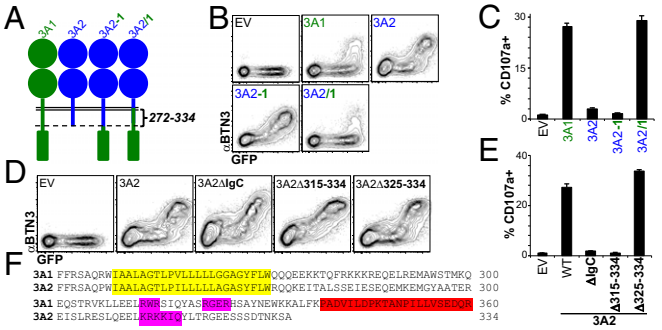

Fig. 4. Motifs regulating BTN3 surface expression and function. (*A*) Wild-type and BTN3A1/3A2 chimaeras used to transfect CRA123 cells, pulsed with 5 μM Zol. (*B*) Expression was monitored by flow cytometry on a fraction of the samples, whereas the residual (*C*) was coincubated with Vγ9Vδ2$^+$ cells and assayed as described for Fig. 3. (*D*) CRA23 cells were transfected with the indicated WT or deletion mutants of BTN3A2; expression was monitored by flow cytometry on a fraction of the samples, whereas the residual (*E*) were treated as in *C*. Data are means of three stimulations ± SD. Representative of three independent experiments. (*F*) Partial amino acid sequences of BTN3A1 (241–360) and BTN3A2 (241–334). TM domains, yellow; start of BTN3A1 B30.2 domain, red; putative ER association motifs, purple.

Discussion

This study has provided many insights into how BTN and BTNL proteins regulate γδ cell biology. First, CR-mediated gene deletion

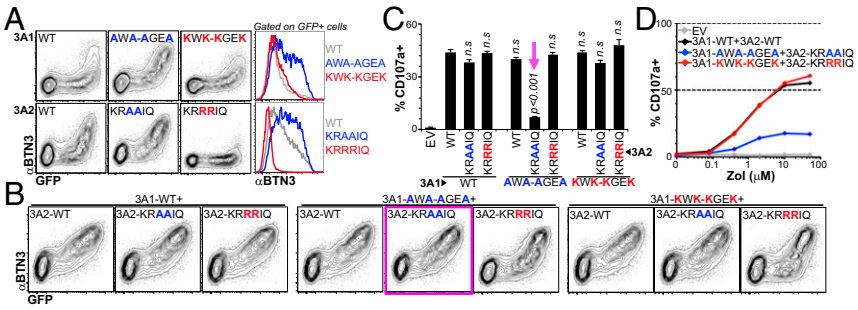

Fig. 6. ER association of BTN3 is critical for its function. (*A*) CRA123 cells were transfected with the indicated WT or ER-retention motif mutants of BTN3A1 (*Upper*) and BTN3A2 (*Bottom*), and cell surface expression assessed by flow cytometry. Representative of three independent transfections. (*B*) CRA123 cells were cotransfected with the indicated constructs before treatment with 5 μM Zol. Cell surface BTN3A expression was monitored and (*C*) the functional potential of the transfectants measured as described for Fig. 4. Data are the mean of three stimulations ± SD. Representative of three independent experiments. *P* values are relative to the combination of WT BTN3A1+BTN3A2. Purple arrow in *C* denotes functional deficiency of cells whose BTN3A expression is shown in purple-boxed plot in *B*. (*D*) CRA123 cells were transfected with pCSIGPW, either as an EV or encoding indicated BTN3 WT or ER motif mutants before a 12-h treatment with Zol (0.04–50 μM, 5× dilution steps) and assayed for their capacity to promote Vγ9Vδ2$^+$ T cell degranulation. Data points are the mean of duplicate stimulations and representative of two independent experiments.

(rather than shRNA knock-down) provided unequivocal evidence that specifically disrupting *BTN3A2* profoundly impaired the capacity to mediate PAg-dependent Vγ9Vδ2$^+$ T cell activation. Moreover, BTN3A2 could be stoichiometrically coimmunoprecipated with BTN3A1, consistent with their forming heteromeric complexes. Although the requirement for *BTN3A2* was not absolute, this likely reflected partial compensation by BTN3A3, which could also be coimmunoprecipitated with BTN3A1. Indeed, *BTN3A1*$^+$ cells lacking *BTN3A2* and *BTN3A3* showed no residual functional activity. Moreover, in experiments in which the functional potentials of *BTN3A*-null CRA123 cells were rescued with *BTN3* genes, potencies (E_{max}) comparable to wild-type cells were achieved only when *BTN3A1* was expressed with *BTN3A2* and/or *BTN3A3*. Nonetheless, because *BTN3A3* was not ordinarily required for Vγ9Vδ2$^+$ T cell activation in cells expressing *BTN3A1* and *BTN3A2*, this study has focused on BTN3A1 and BTN3A2 cooperation.

Optimal Vγ9Vδ2$^+$ T cell responses to a range of Zol concentrations depended on the BTN3A2-IgC domain required for BTN3A2 to interact with BTN3A1, thereby linking complex formation with function. Complex formation was also linked to increased BTN3A1 cell surface expression, although this alone could not explain functional collaboration, as unrestricted surface expression habitually decreased function. Instead, functionally important domains were mapped to intracellular regions of BTN3A1 and BTN3A2 that regulated the proteins' association with the ER. This may have been overlooked by studies employing GFP-fusion proteins because BTN3A1 proteins with altered C-termini can show atypical subcellular localization. In contrast, the importance of ER association was highlighted by a clear instance of functional complementation in which optimal Vγ9Vδ2$^+$ T cell stimulation requires ER retention motifs in either BTN3A1 or BTN3A2 but not both. This is most readily explained by the bioactive unit being a physically associated BTN3A1-3A2 heteromer.

Thus, we propose a model whereby the BTN3A1 ectodomain and B30.2-domains are active entities in Vγ9Vδ2$^+$ cell stimulation, with which BTN3A2 collaborates by regulating the appropriate routing, kinetics, and/or stability of BTN3A1. This may include a critical "dwell time" in the ER, mediating a quality control step for multimer formation, and/or permitting interaction with other moieties (e.g., cargo). Of note, sterol metabolism, which BTN3A1 may monitor via isopentenylpyrophosphate binding, involves ER-resident enzymes of the mevalonate pathway that are regulated by sterol regulatory element-/binding protein factors whose inactive forms also reside in the ER (24). Possibly, the BTN3A1-3A2 heteromers promote ER exit by masking the ER retention motifs, as has been reported in other systems (25). The partial rescue of CRA123 cells by *BTN3A1* likely reflects some capacity of overexpressed homomeric BTN3A1 to exit the ER without BTN3A2/BTN3A3, but its suboptimal routing, kinetics, and/or stability result in suboptimal EC_{50}, and possibly reduced E_{max}. Likewise, the model predicts the observed functional deficits of constructs that accelerate surface expression at the expense of ER association. Of note, BTN3A1 lacks the extended C-terminal sequences of BTN3A3 that promote efficient cell surface BTN3A3 expression.

Our study also establishes parallels of BTN3A1/BTN3A2 biology with Btnl1/Btnl6 and BTNL3/BTNL8 that respectively regulate murine and human gut γδ cells. In each case, optimal function required pairs of proteins that intrinsically displayed ER association, thereby limiting cell surface expression until coexpressed (19). Furthermore Skint1, on which murine Vγ5$^+$ intraepidermal T cells depend, also shows poor surface expression and is functionally ablated by constructs that drive it to the cell surface (26). Hence, our current study emphasizes conserved cellular and molecular mechanisms that may underpin γδ cell regulation across mouse and human, and across peripheral tissues and blood. This is a major departure from the long-held view that human lymphoid γδ cells and murine tissue-resident γδ cells are broadly dissimilar.

Nonetheless, each subtype of γδ cell regulation may have unique signatures. In particular, no equivalent of PAgs has been identified for *BTNL/Btnl*-dependent gut γδ cells or for *Skint1*-dependent murine skin γδ cells. Conversely, although no broadly accepted evidence currently exists that BTN3A1-3A2 present PAg cargo to γδ T cells, our model for BTN3A1-3A2 function has possible parallels with ER dwell times required for CD1d, MHC-I, and MR1 proteins to acquire low-molecular-mass lipid, peptide, and vitamin B metabolite cargoes, respectively. Indeed, those cargoes stabilize the proteins and regulate their cell-surface display to T cells (27–29). Moreover, the actions of different BTN/BTNL gene products may also have parallels with antigen activation of human T cells by MHC class II DQ and DR molecules, for which the closely related molecules, DO and DM, are not absolutely required, but are important in regulating the quality of antigen presentation.

Materials and Methods

All reagents, cells, culture conditions, plasmids, and primers are listed in the *SI Materials and Methods*.

Generation of CR Lines, Cloning, and RT-PCR. Targeting sequences were cloned using short complementary oligos (Table S1). 293T CR lines were generated by transient transfection of pLG2C and single-cell sorting on the basis of GFP expression at 72 h. Tagged constructs were generated by overlapping PCR except mCherry-Sec61β (gift from Professor Martin-Serrano, KCL). Murine FLAG-Btnl1 and HA-Btnl6 and human FLAG-BTNL3 and FLAG-BTNL8 were described (19). Wild-type BTN1A1, BTN2A1, BTN2A2, BTN3A1, BTN3A2, and BTN3A3 were cloned from 293T cells, and wild-type BTNL3, BTNL8S, and BTNL8 from Caco-2 cells (primers in Table S2). Gene expression was checked by RT-PCR, using the same primers.

Flow Cytometry, Confocal Microscopy, and Image Cytometry. 293T cells were seeded at 0.5 × 10^5 per well in 12-well plates and transfected the next day with 1 μg total plasmid DNA before expression assessment by flow, confocal imaging, and image cytometry.

Flow Cytometry. Cells were washed in FACS buffer (FB; PBS, 5% FCS), stained with the indicated antibodies (45 min, 4 °C), washed twice, and resuspended in FB. Data were acquired on a FACSCanto II (BD) and analyzed in FlowJo. For intracellular staining, see following.

Confocal Microscopy. Cells were transferred 24 h posttransfection onto 13-mm glass coverslips, left to adhere for 24 h (37 °C, 5% CO_2), washed with PBS and fixed with CellFix buffer (BD), permeabilized (or not) with permeabilization/wash buffer (PWB; eBioscience), stained in FB (surface) or PWB (intracellular), and washed twice in FB or PWB and then twice in FB. Coverslips were mounted using Prolong Gold (Thermo Fisher). Data were acquired on a TCS SP2 AOBS microscope (HCX PL APO CS 63.0×/1.4 oil objective; Leica) and analyzed in ImageJ.

Image Cytometry. Cells were fixed and permeabilized and stained in PWB supplemented with DAPI. Data were acquired on an ImageStreamX (Merck Millipore) and analyzed in IDEAS. Data were analyzed in IDEAS, and histograms generated in R.

CD107a Assay. Briefly, 293T cells (24 h posttransfection when relevant) were pretreated or not for 12 h with HMBPP or Zol, washed twice in DMEM, coincubated for 5 h with Vγ9Vδ2$^+$ T cells (3:1 ratio) and PE anti-CD107a antibody (1 μg/mL) in RPMI complete media (37 °C, 5% CO_2), washed with FB and stained with AlexaFluor647 anti-CD3 and FITC anti-TCRVδ2, and washed twice and resuspended in FB for acquisition (30).

Coimmunoprecipitation and Western Blotting. 293T cells were seeded at 1×10^6 per well in six-well plates, transfected the next day with 2 μg total plasmid DNA, washed in PBS 48 h posttransfection, and harvested in 0.5 mL lysis buffer [50 mM Tris·HCl at pH 7.4, 150 mM KCl, 10 mM $MgCl_2$, 1 mM $CaCl_2$, 0.5% Nonidet P-40, 0.1% digitonin, 5% glycerol, Complete Protease inhibitor (Roche Diagnostics)]. Lysates were clarified at 12,000 × *g* (4 °C, 5 min), 50 μL mixed with Laemmli buffer, and boiled for input analysis. Remaining lysates were incubated for 4 h at 4 °C on a rotating wheel with 50 μL protein G Dynabeads (Thermo Fisher) preincubated with anti-FLAG antibody and washed three times in lysis buffer. Proteins were eluted in 30 μL Laemmli and analyzed by SDS/PAGE and Western blotting. Blots were visualized by ImageQuant using HRP-anti-HA (3F10; Roche) and HRP-anti-FLAG (M2; Sigma), and by Li-cor Odyssey imaging using rabbit anti-HSP90 (H-114; Santa Cruz Biotechnology) and IRDye680LT anti-rabbit antibodies (Li-cor).

Mass Spectrometry. Anti-FLAG immunoprecipitation (*Coimmunoprecipitation and Western Blotting*) was performed on 5×10^6 CRA123 cells transduced with an empty vector control (EV), FLAG-BTN3A1+HA-BTN3A2, and FLAG-BTNL3+HA-BTNL8. Eluted proteins were subjected to SDS/PAGE until the running front had migrated 1 cm into the gel. Proteins were in-gel digested using trypsin, and peptides were analyzed with an Orbitrap-Fusion Lumos mass spectrometer coupled to an Ultimate3000 HPLC equipped with an EASY-Spray nanosource (Thermo Fisher Scientific). Raw data for triplicate runs were processed using MaxQuant v1.6.0.1, using label-free quantification (MaxLFQ) selected as the quantification algorithm. The proteingroup.txt output table was imported into Perseus software for further processing. LFQ intensities were log2 transformed, and the dataset was filtered for proteins having at least three values in at least one group (each group consisting of triplicate injections). The remaining missing values were imputed using default Perseus settings by drawing from a simulated noise distribution with a down shift of 1.8 and a width of 0.3 compared with the log2 LFQ intensity distribution. Two-sample Welch *t* tests were performed with a permutation-based FDR set at 0.05.

Statistics. Data were analyzed using unpaired two-tailed Student's *t* test. Reference datasets used to determine significance are indicated in each case.

ACKNOWLEDGMENTS. We thank Professor S. J. Neil and Professor J. Martin-Serrano and Dr. C. Swanson (King's) for reagents and discussions; Dr. D. Ushakov and Dr. P. J. Chana (King's) for advice on confocal microscopy and image cytometry; Dr. S. Kjaer and Dr. A. Borg (Crick) for technical assistance; and the flow cytometry units of the Peter Gorer Department of Immunobiology and Guy's Hospital Biomedical Research Centre for technical support. This work is a contribution of the Cancer Research UK (CRUK) King's College Cancer Centre and Immunology Accelerator (CITA). This work was supported by Wellcome Trust Grants [106292/Z/14/Z and 100156/Z/12/Z (to A.C.H.) and 106223/Z/14/Z (to M.H.M.)]; grants and facilities were provided to A.C.H. by the Francis Crick Institute, which receives its core funding (FC001093) from CRUK, the UK Medical Research Council, the National Institute for Health Research Biomedical Research Centre at Guy's, and St. Thomas' NHS Trust and King's College.

1. Hayday AC, et al. (1985) Structure, organization, and somatic rearrangement of T cell gamma genes. *Cell* 40:259–269.
2. Brenner MB, et al. (1986) Identification of a putative second T-cell receptor. *Nature* 322:145–149.
3. Hayday A, Vantourout P (2013) A long-playing CD about the γδ TCR repertoire. *Immunity* 39:994–996.
4. Vantourout P, Hayday A (2013) Six-of-the-best: Unique contributions of γδ T cells to immunology. *Nat Rev Immunol* 13:88–100.
5. Jameson JM, Cruz J, Costanzo A, Terajima M, Ennis FA (2010) A role for the mevalonate pathway in the induction of subtype cross-reactive immunity to influenza A virus by human gammadelta T lymphocytes. *Cell Immunol* 264:71–77.
6. Laezza C, et al. (2015) p53 regulates the mevalonate pathway in human glioblastoma multiforme. *Cell Death Dis* 6:e1909.
7. Harly C, et al. (2012) Key implication of CD277/butyrophilin-3 (BTN3A) in cellular stress sensing by a major human γδ T-cell subset. *Blood* 120:2269–2279.
8. Perfetto L, et al. (2013) Exploring the diversity of SPRY/B30.2-mediated interactions. *Trends Biochem Sci* 38:38–46.
9. Palakodeti A, et al. (2012) The molecular basis for modulation of human Vγ9Vδ2 T cell responses by CD277/butyrophilin-3 (BTN3A)-specific antibodies. *J Biol Chem* 287: 32780–32790.
10. Vavassori S, et al. (2013) Butyrophilin 3A1 binds phosphorylated antigens and stimulates human γδ T cells. *Nat Immunol* 14:908–916.
11. Wang H, et al. (2013) Butyrophilin 3A1 plays an essential role in prenyl pyrophosphate stimulation of human Vγ2Vδ2 T cells. *J Immunol* 191:1029–1042.
12. Sandstrom A, et al. (2014) The intracellular B30.2 domain of butyrophilin 3A1 binds phosphoantigens to mediate activation of human Vγ9Vδ2 T cells. *Immunity* 40: 490–500.
13. Rhodes DA, et al. (2015) Activation of human γδ T cells by cytosolic interactions of BTN3A1 with soluble phosphoantigens and the cytoskeletal adaptor periplakin. *J Immunol* 194:2390–2398.
14. Gu S, et al. (2017) Phosphoantigen-induced conformational change of butyrophilin 3A1 (BTN3A1) and its implication on Vγ9Vδ2 T cell activation. *Proc Natl Acad Sci USA* 114:E7311–E7320.
15. Salim M, et al. (2017) BTN3A1 discriminates γδ T cell phosphoantigens from non-antigenic small molecules via a conformational sensor in its B30.2 domain. *ACS Chem Biol* 12:2631–2643.
16. Lewis JM, et al. (2006) Selection of the cutaneous intraepithelial gammadelta+ T cell repertoire by a thymic stromal determinant. *Nat Immunol* 7:843–850.
17. Boyden LM, et al. (2008) Skint1, the prototype of a newly identified immunoglobulin superfamily gene cluster, positively selects epidermal gammadelta T cells. *Nat Genet* 40:656–662.
18. Turchinovich G, Hayday AC (2011) Skint-1 identifies a common molecular mechanism for the development of interferon-γ-secreting versus interleukin-17-secreting γδ T cells. *Immunity* 35:59–68.
19. Di Marco Barros R, et al. (2016) Epithelia use butyrophilin-like molecules to shape organ-specific gammadelta T cell compartments. *Cell* 167:203–218.e217.
20. Gober HJ, et al. (2003) Human T cell receptor gammadelta cells recognize endogenous mevalonate metabolites in tumor cells. *J Exp Med* 197:163–168.
21. St-Louis É, et al. (2017) Involvement of the coatomer protein complex I in the intracellular traffic of the delta opioid receptor. *Mol Cell Neurosci* 79:53–63.
22. Teasdale RD, Jackson MR (1996) Signal-mediated sorting of membrane proteins between the endoplasmic reticulum and the golgi apparatus. *Annu Rev Cell Dev Biol* 12: 27–54.
23. Peigné CM, et al. (2017) The juxtamembrane domain of butyrophilin BTN3A1 controls phosphoantigen-mediated activation of human Vγ9Vδ2 T cells. *J Immunol* 198: 4228–4234.
24. Mullen PJ, Yu R, Longo J, Archer MC, Penn LZ (2016) The interplay between cell signalling and the mevalonate pathway in cancer. *Nat Rev Cancer* 16:718–731.
25. Michelsen K, Yuan H, Schwappach B (2005) Hide and run. Arginine-based endoplasmic-reticulum-sorting motifs in the assembly of heteromultimeric membrane proteins. *EMBO Rep* 6:717–722.
26. Barbee SD, et al. (2011) Skint-1 is a highly specific, unique selecting component for epidermal T cells. *Proc Natl Acad Sci USA* 108:3330–3335.
27. Brozovic S, et al. (2004) CD1d function is regulated by microsomal triglyceride transfer protein. *Nat Med* 10:535–539.
28. Park B, et al. (2006) Redox regulation facilitates optimal peptide selection by MHC class I during antigen processing. *Cell* 127:369–382.
29. McWilliam HE, et al. (2016) The intracellular pathway for the presentation of vitamin B-related antigens by the antigen-presenting molecule MR1. *Nat Immunol* 17: 531–537.
30. Betts MR, et al. (2003) Sensitive and viable identification of antigen-specific CD8+ T cells by a flow cytometric assay for degranulation. *J Immunol Methods* 281:65–78.
31. Pertel T, et al. (2011) TRIM5 is an innate immune sensor for the retrovirus capsid lattice. *Nature* 472:361–365.
32. Cong L, et al. (2013) Multiplex genome engineering using CRISPR/Cas systems. *Science* 339:819–823.